Nonuniform Grid based Lattice Boltzmann Method for Numerical Simulation of Glow Discharge Plasma in Argon

Yong-Jun Kim[1*], Ji-Hyok Kim[2], Song-Nam Kwon[3], Myong-Song Ro[4]

[1,2,3] Faculty of Physical Engineering, Kim Chaek University of Technology, Pyongyang 999003, Democratic People's Republic of Korea

[4]Department of Information, SinUiJu Cha Kwang Su University of Education, Sinuiju, Democratic People's Republic of Korea

Abstract

Plasma parameters of argon dc glow discharge at 1torr pressure are numerically analyzed. Governing equations are based on the drift-diffusion theory and solved by lattice Boltzmann method (LBM) and finite difference method (FDM). The LBM is employed on non-uniform grid, which is checked by simulating lid-driven cavity flow. Analysis of glow discharge with fixed temperatures for plasma species is performed for comparison between the results on the uniform grid and on the non-uniform one. The results show that the latter is required less computational cost than the former. The simulation of glow discharge is performed with temperature field, whose results are in good agreement with those from the experiments and by COMSOL.

Keywords: Glow discharge, Lattice Boltzmann method, Non-uniform grid, Multi-field, Computational fluid dynamics.

1. Introduction

Most practical plasmas, including arc discharge and glow discharge, are weakly ionized plasmas under non-equilibrium condition. That is, the temperatures of the heavy species and the electrons are not the same ($T_e >> T_i$). In addition, the temperature distributions of the species are also not uniform inside the discharge tube, which are necessary in order to account for energy conversion, such as optical and thermal phenomena, ionization, excitation, etc.

In the past, there have been many efforts to analyze the parameter distributions of non-equilibrium glow discharge plasma. Rafatov et al. (2007) assumed that the temperatures of electrons and ions are constant and led the similar density distributions as the experimental results through the simulation

*Corresponding Author Email: kyj801031@star-co.net.kp

Published: 20/10/2025

DOI: https://doi.org/10.70558/IJST.2025.v2.i4.241091

for the charged species only in the density field. Also, many works (Fu et al., 2011; Fu et al., 2014; Mahadevan & Raja, 2010) carried out in the multiple fields with the consideration of the temperature field, most of which assumed only the temperature of the heavy species to be constant. However, Tereshonok (2014) assumed only the electron temperature to be constant and solved the energy equation for the heavy species. It is expected that these works made the different assumptions due to the various discharge conditions.

The development of computational techniques improves the accuracy and stability of numerical simulations and makes them easier. Recently, the LBM has emerged as a powerful tool for computational fluid dynamics (CFD) analysis due to its advantages, such as relatively simple numerical structure, easy boundary processing, convenient parallel computation, etc. It has been widely used for not only fluid flow simulations, such as advection-diffusion flow (Dapelo et al., 2021) and convection heat transfer (Wang et al., 2022), compressible flow (Wilde et al. 2020) and multiphase-multicomponent flow (Fogliatto et al., 2021; Xue et al., 2020), but also plasma researches (Huang et al., 2024; Djebali et al., 2014) and radiative heat transfer (Patidar et al., 2017). Since the plasma simulations are performed in the multi-field, they take high storages and computational costs. To avoid this difficulty, nonuniform grid based lattice Boltzmann method (NLBM) (Fakhari & Lee, 2015; Mondal & Mishra, 2008) are employed, which showed its advantages in a variety of benchmark problems. The key advantage is that detailed information in the region where large gradients of parameters exist can be obtained with low computational cost. The NLBMs have been used in many CFD models such as heat conduction (Mishra et al., 2009) and natural convection (Kuznik et al., 2007).

In the present work, we establish a mathematical model for the densities and temperatures of the species and simulate by using the NLBM. It is the aim of this work to obtain more accurate results with the low computational costs for the plasma simulations.

We begin by explaining the NLBM in Sect. 2.1. Then, in Sect. 2.2, we establish the governing equations for the fields of density and temperature in the glow discharge plasma, whose detailed physical parameters are given in Sect. 2.3. In Sect. 2.4, we also describe the macroscopic boundary conditions and the corresponding microscopic boundary conditions for LBM. We give the simulation results and their explanations in Sect. 3, and finally, in Sect. 4, we summarize the conclusions.

2. Numerical model

2.1. LBM on non-uniform grid

The NLBMs are provided in several works (Fakhari & Lee, 2015; Mondal & Mishra, 2008; Mishra et al., 2009; Kuznik et al., 2007), which describe the connection between the fine grid and the coarse one in different ways. We construct the following model based on the mathematical model of Fakhari & Lee (2015) for the simplification of the simulation.

2.1.1. Mesh refinement and interpolation

In contrast to the previous work (Fakhari & Lee, 2015) the fine grid for the glow discharge must be applied to the boundary layers because of the existing sharp change of parameters near them. The computation region and the grid refinement are shown in Figure. 1. The tube length is L=30cm and the tube radius is R=3cm. Here, the thicknesses of the fine layers are chosen to be 5mm and 2mm for the anode layer and walls, respectively, and 10 mm for the cathode layer. Also, the ratio between the sizes of the fine and the coarse grids is set to 2.

Interpolation is applied for the connection between the coarse grid and the fine one. The influence of the fine grid on the coarse grid can be directly obtained from the distribution functions at the fine grid points corresponding to the coarse grid. However, for the influence of the coarse grid on fine grid, we use the linear interpolation at the coarse-fine boundaries. For example, in Figure 1, some distribution functions (k=3, 7, 6) on point **B** directions are unknown but ones on points **A** and **C** are known. Hence, we can obtain them as follows,

$$f_k^{\mathrm{B}} = \frac{f_k^{\mathrm{A}} + f_k^{\mathrm{C}}}{2}$$

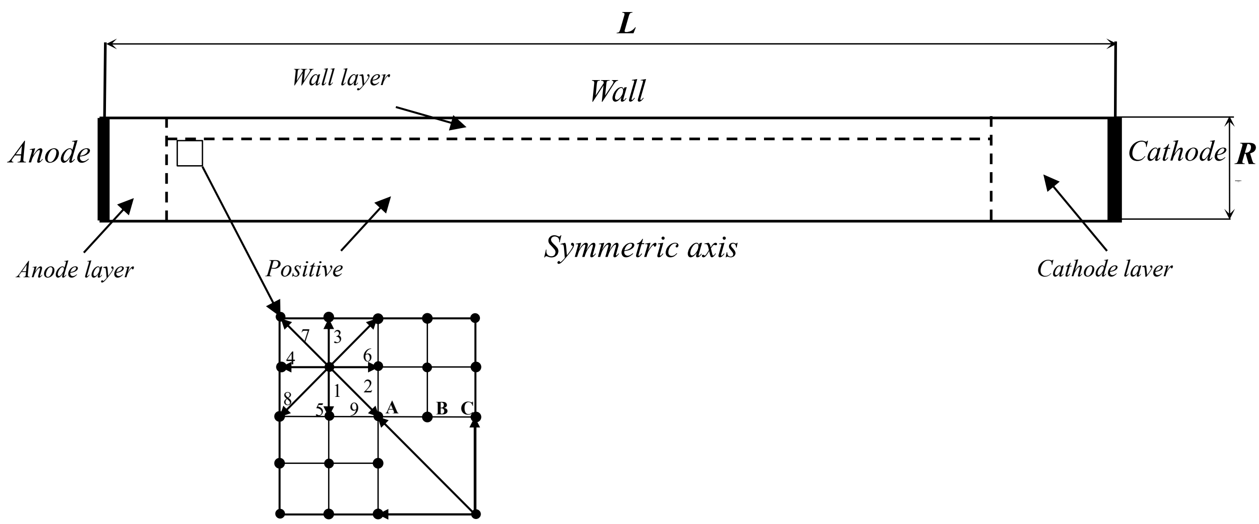

Figure. 1. Computational region for LB simulation of glow discharge. (Fine grids: Wall, Anode and Cathode layers. Coarse grid: Positive column).

2.1.2. Lattice Boltzmann Model

The governing equations for glow discharge consist of the advection-diffusion equations for scalar quantities such as temperature, concentration and density.

$$\frac{\partial \rho(\bar{x},t)}{\partial t} + \bar{u}(\bar{x},t)\nabla \rho(\bar{x},t) = D(\bar{x},t)\Delta\rho(\bar{x},t) + S(\bar{x},t), \tag{1}$$

where $\rho(\bar{x},t)$, $\bar{u}(\bar{x},t)$, $D(\bar{x},t)$ and $S(\bar{x},t)$ denote the density, the velocity, the diffusion coefficient and the source term at time t and position $\bar{x}$, respectively.

The discretized LB equation with the source term can be expressed as follows,

$$\text{Collision: } f_k^*(\bar{x},t) = f_k(\bar{x},t) - \frac{\Delta t}{\tau}(f_k(\bar{x},t) - f_k^{eq}(\rho,\bar{u})) + S_k(\bar{x},t)\Delta t, \tag{2}$$

$$\text{Propagation: } f_k(\bar{x} + \bar{c}_k \Delta t, t + \Delta t) = f_k^*(\bar{x},t). \tag{3}$$

In the collision model, $f_k(\bar{x},t)$ represents the distribution function on k-direction at time t and position $\bar{x}$, which is defined in D2Q9 model. Here, the discrete equilibrium distribution functions and the discrete source terms are

$$f_k^{eq}(\bar{x},t) = \rho(\bar{x},t)\omega_k(1 + \frac{\bar{c}_k \cdot \bar{u}(\bar{x},t)}{c_s^2}), \tag{4}$$

$$S_k(\bar{x},t) = (1 - \frac{1}{2\tau})\omega_k S(\bar{x},t). \tag{5}$$

In the D2Q9 model, the discrete speeds and weight factors are

$$\bar{c}_k = \begin{cases} (0,0) & k=1 \\ c(\cos\frac{\pi k}{2}, \sin\frac{\pi k}{2}) & k=\overline{2,5}, \\ \sqrt{2}c(\cos[(2k+1)\frac{\pi}{4}], \sin[(2k+1)\frac{\pi}{4}]) & k=\overline{6,9} \end{cases} \tag{6}$$

$$\omega_k = \begin{cases} 4/9 & k=1 \\ 1/9 & k=\overline{2,5}. \\ 1/36 & k=\overline{6,9} \end{cases} \tag{7}$$

In addition, $c_s = 1/\sqrt{3}c$ represents the speed of sound.

In the propagation model, the distribution functions at the next time step can be obtained from the post-collision distributions $f_k^*(\bar{x},t)$, for which the following interpolation is used (Fakhari & Lee, 2015).

$$f_k(\bar{x},t+\Delta t)=\frac{\sigma(1+\sigma)}{2}f_k^*(\bar{x}+\Delta\bar{x},t)+(1-\sigma^2)f_k^*(\bar{x},t)-\frac{\sigma(1+\sigma)}{2}f_k^*(\bar{x}-\Delta\bar{x},t), \tag{8}$$

where σ is the CFL number defined as $\sigma=|\bar{c}_k|\Delta t/\Delta x_k$. It is expected that the approach could lead to higher convergence by breaking the relationship between the grid time and the grid space in the propagation step.

The density satisfies the following relationship with the distribution functions,

$$\rho=\sum_k f_k+\frac{S\Delta t}{2}. \tag{9}$$

The above-mentioned LBM reaches second-order accuracy in time. The diffusion coefficient, mobility and other variables are discussed in detail in Sect. 2.3.

On the non-uniform grid, the LBM separately operates on the fine grid and coarse one. There is no difference between the two operations in the collision step, but CFLs in the propagation step are different. That is, the above non-uniform process has the advantage of simplifying the operation by using the same dimensionless and computation algorithm for every grid by employing CFL number in the propagation step.

2.2. Governing equations for glow discharge

For the argon glow discharge, four species (ground state atom (**Ar**), excited atom (**Ar***), cation (**Ar^+**) and electron (**e**) are considered, and temperature distribution for the electrons is investigated. The temperature of the heavy species is assumed to be 0.025eV. The chemical reactions between the plasma species are shown in Table. 1.

Table 1. Chemical reactions for argon glow discharge plasma.

No	Reaction	Reaction rate, *k*	Energy change [eV]
R1	$Ar+e \rightarrow Ar^+ + 2e$	$1.27\times10^{-8}T_e^{0.5}[\mathrm{eV}]\exp(-15.76/T_e[\mathrm{eV}])(\mathrm{cm^3/s})$	15.76

R2	Ar+e→Ar*+e	$1\times10^{-11}T_e^{-0.75}\exp(-11.56/T_e)(\mathrm{cm^3/s})$	11.56
R3	Ar*+e→Ar^++2e	$1\times10^{-10}T_e^{0.3}\exp(-4.2/T_e)(\mathrm{cm^3/s})$	4.2
R4	Ar*+e→Ar+e	$8.6\times10^{-10}T_e^{0.74}[\mathrm{eV}](\mathrm{cm^3/s})$	-11.56
R5	Ar^++2e→Ar*+e	$5\times10^{-27}T_e^{-4.5}(\mathrm{cm^6/s})$	-4.2
R6	Ar^++e→Ar	$2\times10^{-7}(\mathrm{cm^3/s})$	-15.76
R7	Ar*+Ar*→Ar^++Ar+e	$5\times10^{-10}(\mathrm{cm^3/s})$	-7.36
R8	Ar*+Ar→2Ar	$2.3\times10^{-15}(\mathrm{cm^3/s})$	-11.56

As mentioned above, the glow discharge plasma is a weakly ionized plasma, therefore the density of the ground state species is almost unchanged. Hence, the governing equations can be written for the excited species, the cations and the electrons,

$$\frac{\partial n_s}{\partial t}+\bar{u}_s\nabla n_s=D_s\Delta n_s+R_s, \tag{10}$$

where n_s, $\bar{u}_s$ and D_s represent the number density, the drift velocity and the diffusion coefficient of *s*-species, respectively. The drift velocity is assumed to be linearly dependent on the electric field:

$$\bar{u}_s=\iota_s\mu_s\bar{E}, \tag{11}$$

where μ_s is the mobility of *s*-species, ι_s is set to 1 for the cations, -1 for the electrons, and 0 for the excited species. In addition, R_s represents the production or the loss of the species of interest, which can be expressed by the plasma chemical reactions as follows.

$$R_i=\alpha(|\bar{E}|)|\bar{\Gamma}_e|+k_3n_*n_e-k_5n_in_e^2-k_6n_in_e+k_7n_*n_*, \tag{12}$$

$$R_*=k_2n_nn_e-k_3n_*n_e-k_4n_*n_e+k_5n_in_e^2-2k_7n_*^2-k_8n_*n_n, \tag{13}$$

$$R_e=\alpha(|\bar{E}|)|\bar{\Gamma}_e|+k_3n_*n_e-k_5n_in_e^2-k_6n_in_e+k_7n_*n_*, \tag{14}$$

where '*i*', '*' and '*e*' represent the cations, the excited species and the electrons, respectively, and

k_j is the rate coefficients of the j-th reaction, $\alpha(|\bar{E}|)$ is the Townsend coefficient and $|\bar{\Gamma}_e|$ is the electron flux density,

$$\bar{\Gamma}_e = -n_e \bar{u}_e - D_e \nabla n_e . \tag{15}$$

The electron energy determines by the following electron energy conservation equation,

$$\frac{\partial Q_e}{\partial t} + \bar{u}_e^{\varepsilon} \nabla Q_e = \chi_e \Delta Q_e + G_e , \tag{16}$$

where Q_e is the energy density of the s-species, $\bar{u}_e^{\varepsilon}$ is the energy drift velocity of the electrons, χ_e is the energy diffusion coefficient for the electrons and $G_e = \bar{j} \cdot \bar{E}$ is the energy source term by the Joule heating. The electron temperature is related to the energy density as follows,

$$Q_e = D / 2 \mathrm{k_B} T_e n_e , \tag{17}$$

where D is set to be 2 in two-dimensional.

It can be seen that the heavy species means the ground-state species since its density is about 1e7 times as large as one of the charged or the excited species. Its density is assumed to be $n_h = 3.54e16\mathrm{cm}^{-3}$, which corresponds to 1 torr pressure.

The governing equation for the electric potential is expressed by Poisson’s equation.

$$\Delta \varphi = -\frac{\mathrm{e}(n_i - n_e)}{\varepsilon_0} , \tag{18}$$

where $\mathrm{e} = 1.6 \cdot 10^{-19}\,\mathrm{C}$ and $\varepsilon_0 = 8.85 \cdot 10^{-12}\,\mathrm{C/(V \cdot m)}$.

The relationship between the electric field and the electric potential is

$$\bar{E} = -\bar{\nabla} \varphi . \tag{19}$$

2.3. Physical parameters for glow discharge

Parameters for the density field are provided by Rafatov et al. (2007).

The Townsend coefficient and the cation mobility can be expressed as functions of the reduced electric field as follows,

$$\begin{aligned}\alpha(E/n)/n &= 1.1e-18\exp[-72/(E/n)]+5.5e-17\exp(-187/(E/n)] \\ &+3.2e-16\exp(-700/(E/n))-1.5e-16\exp(-10000/(E/n))\end{aligned}, \tag{20}$$

$$\mu_i[\mathrm{cm}^2/(\mathrm{s}\cdot\mathrm{V})]=\begin{cases}\dfrac{1e3\times(1-2.22^{-3}\cdot E/p)}{p} & E/p\le 60\dfrac{\mathrm{V}}{\mathrm{cm}\cdot\mathrm{torr}} \\ \dfrac{8.25e3}{p\sqrt{E/p}}(1-\dfrac{86.52}{(E/p)^{3/2}}) & E/p>60\dfrac{\mathrm{V}}{\mathrm{cm}\cdot\mathrm{torr}}\end{cases}, \tag{21}$$

where E/n is given in [Td] with $1\mathrm{Td}=10^{17}\,\mathrm{V}\cdot\mathrm{cm}^2$ and $\alpha(E/n)/n$ is $[\mathrm{cm}^2]$. The electron mobility is

$$\mu_e=\frac{3e5}{p}\mathrm{cm}^2/(\mathrm{s}\cdot\mathrm{V}). \tag{22}$$

The diffusion coefficient of the *s*-species is calculated from the mobility by Einstein's relation.

$$D_s=\mu_s T_s, \tag{23}$$

where T_s is the temperature of the *s*-species given in electron volts [eV].

The secondary electron emission coefficient is used as a constant approximation, $\gamma=0.07$.

The parameters for the temperature field are given by the relationship with those for the density field. From the comparison between Eq. (16) and the electron energy equation presented by Pan et al. (2015), we can obtain the following energy mobility and energy diffusion coefficient.

$$\mu_e^{\varepsilon}=\frac{5}{3}\mu_e, \tag{24}$$

$$\chi_e=\mu_e^{\varepsilon}T_e=\frac{5}{3}D_e. \tag{25}$$

2.4. Boundary conditions

Table 2. Boundary condition set for glow discharge plasma.

Boundary	Parameters				
	n_*	n_i	n_e	T_e	φ
Anode	$n_* = 0$	$n_i = 0$	$\partial n_e/\partial \overline{n} = 0$	$\partial T_e/\partial \overline{n} = 0$	$\varphi = 0$
Cathode	$n_* = 0$	$\partial n_i/\partial \overline{n} = 0$	$n_e = F(n_i)$	$\partial T_e/\partial \overline{n} = 0$	$\varphi = -U$
Wall	$\partial n_*/\partial \overline{n} = 0$	$\partial n_i/\partial \overline{n} = 0$	$\partial n_e/\partial \overline{n} = 0$	$\partial T_e/\partial \overline{n} = 0$	$\partial \varphi/\partial \overline{n} = 0$

The boundary conditions for the glow discharge are given in Table. 2, where $\overline{n}$ represents the outward normal vector and $n_e = F(n_i)$ is a secondary electron emission, which has the following form,

$$n_e = F(n_i) = \gamma \frac{\mu_i}{\mu_e} n_i . \tag{26}$$

$\mathrm{U} = 400\mathrm{V}$ is the applied voltage. As shown in the table, the boundary conditions are the homogeneous Neumann and Dirichlet conditions.

The microscopic boundary conditions are given for unknown microscopic distribution functions as follows,

Microscopic homogeneous Neumann boundary condition: $f_k(x_w,t) = 2f_k(x_f,t) - f_k(x_{ff},t)$, (27)

Microscopic Dirichlet boundary condition: $f_{\bar{k}} = -f_k + 2\omega_k \mathrm{C}$, (28)

where $x_f = x_w - \overline{n}\delta x$, $x_{ff} = x_w - 2\overline{n}\delta x$, $\overline{c}_k = -\overline{c}_{\bar{k}}$, and C is the constant of the macroscopic Dirichlet boundary condition.

3. Results and Discussion

To verify the NLBM, the lid-driven cavity flow in two dimensions (Sedaghatjoo et al., 2018) and the glow discharge with the fixed species temperatures (Rafatov et al., 2007) are simulated by it.

First, we simulate the two-dimensional lid-driven cavity flow, whose parameters and boundary conditions are as follows, Reynolds number: $\mathrm{Re}=100$, Mesh size: 41×41, Top boundary: $u_x=0.1$ and $u_y=0$,

where the variables are dimensionless parameters. The bounce-back scheme is used for other boundaries,

$$f_k(\bar{x},t)=f_{\bar{k}}(\bar{x},t).$$

The velocity distribution is shown in Figure.2. As shown in the figure, the results by the NLBM are similar to ones by boundary elements method (Sedaghatjoo et al., 2018) and identical with ones by the LBM on the uniform grid. Also, the NLBM has an advantage in computational cost as mentioned above.

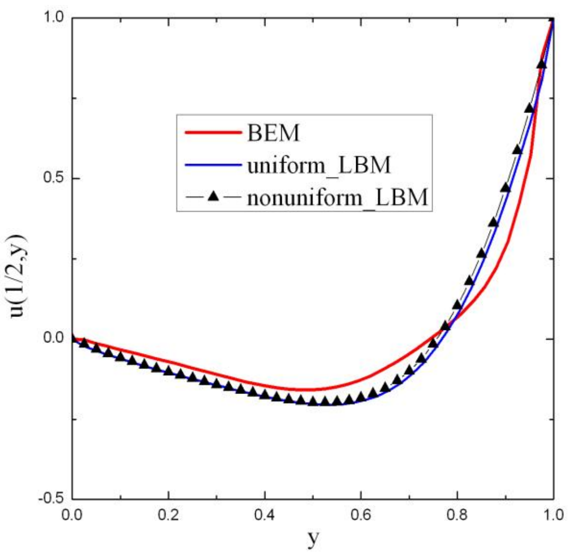

(a). Comparison between results by various computation methods.

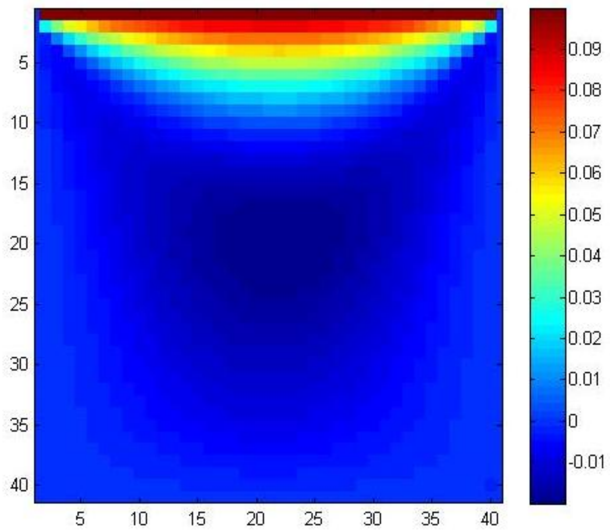

(b). 2D velocity distribution of Lid-cavity flow simulation by NLBM.

Figure. 2. Simulation of lid driven cavity flow.

Second, the analysis for glow discharge with the fixed temperatures is performed for the verification, and the detailed parameters are provided in Sect. 2.3.

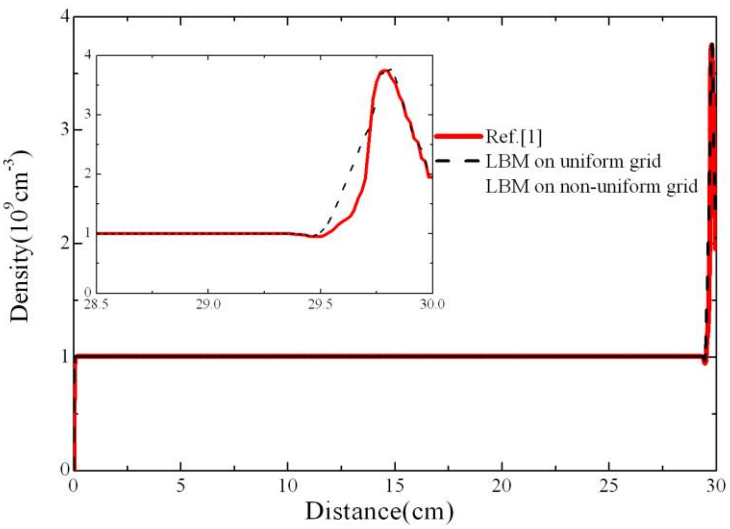

(a). Ion densities.

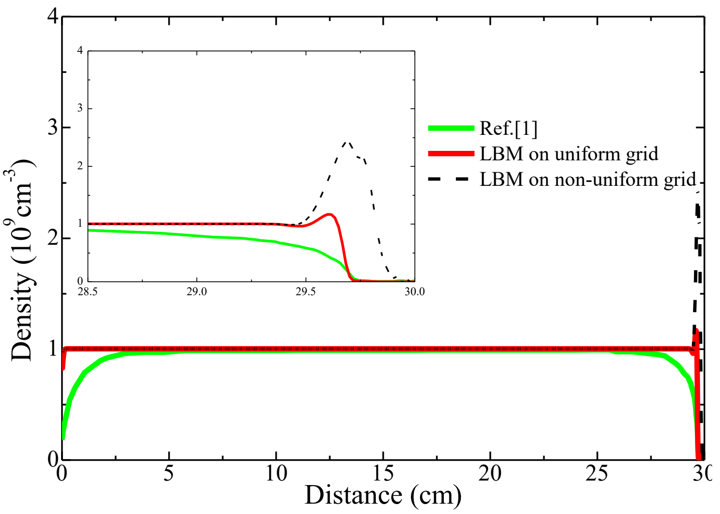

(b). Electron densities.

Figure. 3. Charged densities derived by various numerical methods in Case 1 presented by Rafatov et al. (2007).

Figure.3 shows the results, (a) ion densities, (b) electron densities. For simulation, the boundary conditions for the species density and the electric potential given in Table. 2 are applied, and the temperatures of the electrons and the heavy species are assumed to be constants, T_e=1eV and T_i=0.025eV. The parameter distributions in density field reveal the tendency similarities to those in the previous works including the rapid increase of ion density (up to $3.71\times10^{15}\,\mathrm{m}^{-3}$) near the cathode, the presence of relatively low electron density and the sharp decrease of electrical potential due to the formation of sheath layer, etc. The thickness of the sheath layer is about 5 mm, which is in agreement with the results of Rafatov et al. (2007). Hence we fix the thickness of the fine layer near the cathode at 10 mm as in Sect. 2.1.1 to reduce the error from rapid change of parameters at the boundary between the fine and the coarse grids. The operation by the present model is performed with low computational cost (1.5 times less than on the uniform grid in memory).

The above comparisons have fully shown the advantages of non-uniform grid over uniform one, which means that it may avoid the difficulty of the operation in multi-field simulations. From the above results, our model seems to be successfully applied to the fluid flows and the plasma simulations, and therefore it may be employed for the more complex simulations.

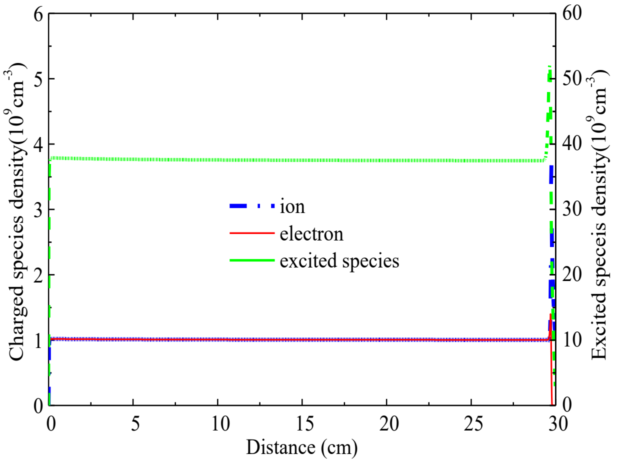

(a). Species density distributions.

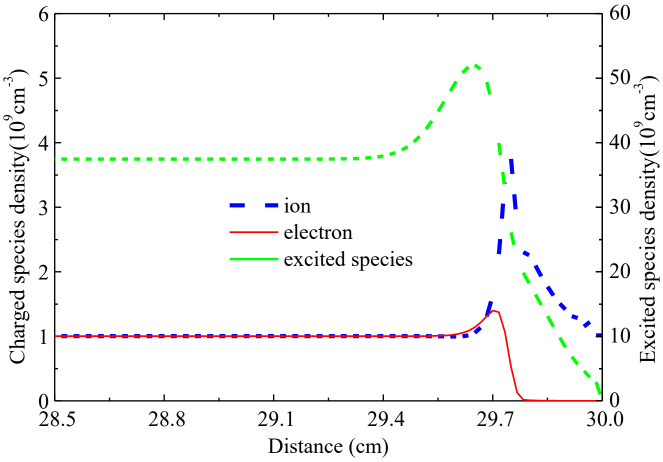

(b). Species density distributions (zoom of the data plotted in panel (a)).

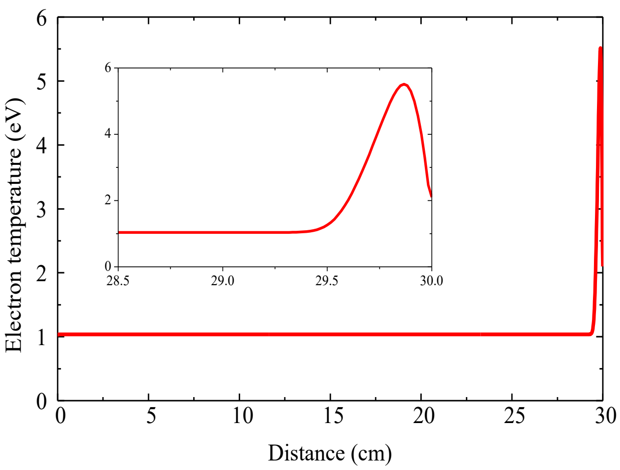

(c). Electron temperature distribution.

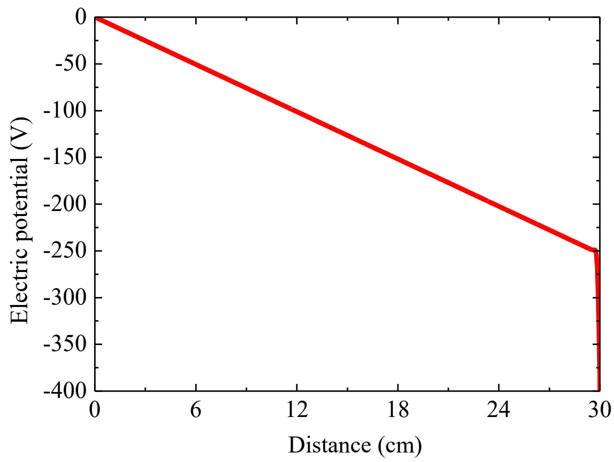

(d). Electric potential.

Figure. 4. Glow discharge simulation considering the non-uniform temperature field.

Figure. 4 shows the simulation results by using NLBM in the multiple fields (the density field, the temperature field and the electric field). For the electron temperature, it exhibits good agreement with the results of Fu et al. (2014). The electron temperature in the positive column is about 1.03eV and increases to a maximum 5.5eV in the sheath layer. This seems to be because the Joule heat in the sheath layer is larger than in the positive column due to the strong electric field. The sharp decrease of the electrical potential in the sheath layer appears from about -240V. Also, the electric current is about 2mA, which is similar to 2.3mA of Rafatov et al. (2007). However, the results show the linearity of the species densities unlike those of Fu et al. (2014). It seems to be caused by the influences of the walls. Rafatov et al. (2007) are applied the homogeneous Neumann condition to the walls from the fact that the effect of walls is weak at the inner regions since the discharge tube is long. In contrast with that, Fu et al. (2014) considered that the species are annihilated instantly when collide with the walls. We will verify about this in following study. Other parameters are similar to the previous works (Rafatov et al., 2007; Fu et al., 2014).

4. Conclusions

We establish a mathematical model based on the drift-diffusion theory, which takes into account the four species and eight chemical reactions for glow discharge and is simulated by using the NLBM. Through the two-dimensional simulation of the lid-driven cavity flow and the analysis for the glow discharge with the fixed species temperatures, we verify our mathematical model, and emphasize its advantages in NLBM application to the multiple fields. Reducing the computational cost, the results of the glow discharge analysis combining with the temperature field are in good agreement with the previous results. The present model can be used for the other plasma simulations such as the arc and DB discharges.

On the other hand, the use of the square elements is restricted by the computational cost in large computational domain size since the element number depends linearly on the domain size. This may be overcome by combining with finite element method (Baroudi & Lee, 2021) or meshless method (Miotti et al., 2021). Our future work will carry out the plasma simulations by using such LBMs.

References

[1] Rafatov, I.R., Akbar, D., & Bilikmen, S. (2007). Modelling of non-uniform DC driven glow discharge in argon gas. *Physics Letters A*, 367, 114–119.

[2] Fu, P., Qian, Y.-J., Song, S.-t., Ding, K., & Shi, J.-J. (2011). Development of Numerical Model for Radio Frequency Atmospheric Pressure Glow Discharges in Argon. *Journal of Donghua University*, 28, 391-395.

[3] Fu, Y., Luo, H., Zou, X. & Wang, X. (2014). Research on Similarity Law of Glow Discharge in Argon at Low Pressure by Numerical Simulation. *IEEE Transactions on Plasma Science*, 42, 1544-1551.

[4] Mahadevan, S., & Raja, L.L. (2010). Simulations of direct-current air glow discharge at pressures 1

Torr: Discharge model validation. *Journal of Applied Physics*, 107, 093304.

[5] Tereshonok, D.V. (2014). Numerical Simulation of Surface Glow Discharge in Molecular Nitrogen. *Plasma Investigations*, 52, 352–356.

[6] Dapelo, D., Simonis, S., Krause, M.J., & Bridgeman, J. (2021). Lattice-Boltzmann coupled models for advection–diffusion flow on a wide range of Péclet numbers. *Journal of Computational Science*, 51, 101363.

[7] Wang, C.-H., Liu, Z.-Y., Jiang, Z.-Y., & Zhang, X.-X. (2022). Numerical investigations of convection heat transfer in a thermal source-embedded porous medium via a lattice Boltzmann method. *Case Studies in Thermal Engineering*, 30, 101758.

[8] Wilde, D., Krämer, A., Reith, D., & Foysi, H. (2020). Semi-Lagrangian lattice Boltzmann method for compressible flows. *Physical Review E*, 101, 053306.

[9] Fogliatto, E.O., Clausse, A., & Teruel, F.E. (2021). Assessment of a double-MRT pseudopotential lattice Boltzmann model for multiphase flow and heat transfer simulations. *International Journal of Thermal Sciences*, 159, 106536.

[10] Xue, X., Biferale, L., Sbragaglia, M., & Toschi, F. (2020). A lattice Boltzmann study on Brownian diffusion and friction of a particle in a confined multicomponent fluid. *Journal of Computational Science*, 47, 101113.

[11] Huang, H., Jin, K., Li, K., & Zheng, X. (2024). Modeling of nonequilibrium effects in a compressible plasma based on the lattice Boltzmann method. *Physics of Plasmas*, 31, 093902.

[12] Djebali, R. (2014). Investigating Plasma Jets Behavior using Axisymmetric Lattice Boltzmann Model under Temperature Dependent Viscosity. *Commun. Comput. Phys*, 15, 677-691.

[13] Patidar, S., Kumar, S., Srivastava, A., & Singh, S. (2017). Lattice Boltzmann method-based solution of radiative transfer equation for investigating light propagation through laser-irradiated tissue phantoms. *International Communications in Heat and Mass Transfer*, 84, 144–149.

[14] Fakhari, A., & Lee, T. (2015). Numerics of the lattice boltzmann method on nonuniform grids: Standard LBM and finite-difference LBM. *Computers & Fluids*, 107, 205–213.

[15] Mondal, B., & Mishra, S.C. (2008). Lattice Boltzmann method applied to the solution of the energy equations of the transient conduction and radiation problems on non-uniform lattices. *International Journal of Heat and Mass Transfer*, 51, 68–82.

[16] Mishra, S.C., Mondal, B., Kush, T., & Krishna, B.S.R. (2009). Solving transient heat conduction problems on uniform and non-uniform lattices using the lattice Boltzmann method. *International Communications in Heat and Mass Transfer*, 36, 322–328

[17] Kuznik, F., Vareilles, J., Rusaouen, G., & Krauss, G. (2007). A double-population lattice Boltzmann method with non-uniform mesh for the simulation of natural convection in a square cavity. *International Journal of Heat and Fluid Flow*, 28, 862–870.

[18] Khazaeli, R., Ashrafizaadeh, M., & Mortazavi, S., (2015). A Ghost Fluid Approach for Thermal Lattice Boltzmann Method in Dealing with Heat Flux Boundary Condition in Thermal Problems with Complex Geometries. *Journal of Applied Fluid Mechanics*, 8, 439- 452.

[19] Pan, J., Tan, Z., Wang, X., Nie, L., Sha, C., & Chen, X. (2015). Comparative Study of Pulsed Dielectric Barrier Discharges in Argon and Nitrogen at Atmospheric Pressure. *IEEE Transactions on Plasma Science*, 43, 557-566.

[20] Sedaghatjoo, Z., Dehghan, M., & Hosseinzadeh, H. (2018). Numerical solution of 2D Navier–Stokes equation discretized via boundary elements method and finite difference approximation. *Engineering Analysis with Boundary Elements*, 96, 64–77.

[21] Baroudi, L., & Lee, T. (2021). Simulation of a bubble rising at high Reynolds number with mass-conserving finite element lattice Boltzmann method. *Computers and Fluids*, 220, 104883.

[22] Miotti, D., Zamolo, R., & Nobile, E. (2021). A Fully Meshless Approach to the Numerical Simulation of Heat Conduction Problems over Arbitrary 3D Geometries. *Energies*, 14, 1351.